J. Membrane Biol. 118, 55–67 (1990)

The Journal of
Membrane Biology

Coupling of K^+-Gating and Permeation with Ca^{2+} Block in the Ca^{2+}-Activated K^+ Channel in *Chara australis*

D.R. Laver
School of Biological Sciences, A12, The University of Sydney, Sydney, 2006, Australia.

Summary. The patch-clamp technique is used here to investigate the kinetics of Ca^{2+} block in single high-conductance Ca^{2+}-activated K^+ channels. These channels are detected in the membrane surrounding cytoplasmic drops from *Chara australis*, a membrane which originates from the tonoplast of the parent cell. The amplitudes and durations of single channel events are measured over a wide range of membrane potential (−300 to 200 mV). Ca^{2+} on either side of the channel reduces its K^+ conductance and alters its ion-gating characteristics in a voltage-dependent manner. This Ca^{2+}-induced attenuation of conductance is analyzed using the theory of diffusion-limited ion flow through pores. Interaction of external Ca^{2+} with the channel's ion-gating mechanism is examined in terms of a kinetic model for ion-gating that includes two voltage-dependent gating mechanisms. The kinetics of channel block by external Ca^{2+} indicates that (i) external Ca^{2+} binds at two sites, a superficial site and a deep site, located at 8 and 40% along the trans-pore potential difference, (ii) the external vestibule cannot be occupied by more than one Ca^{2+} or K^+, and (iii) the kinetics of Ca^{2+} binding at the deep site is coupled with that of a voltage-dependent gate on the external side of the channel. Kinetics of channel block by internal Ca^{2+} indicates that more than one Ca^{2+} is involved.

Key Words Ca^{2+} block · diffusion limitation · ion-channel structure

Introduction

Cytoplasmic drops from *Chara australis* are surrounded by a membrane which is believed to be derived from tonoplast (Lühring, 1986; Sakano & Tazawa, 1986). Patch-clamp studies of this membrane have shown high conductance K^+ channels which are also highly selective for K^+ over Na^+ (Lühring, 1986). Their unitary current saturates at high membrane potential and at high K^+ concentration ($[K^+]$) (Laver, Fairly & Walker, 1989). They have two main conductance states (0 and 170 pS in 150 mol/m^3 KCl) as well as several short-lived subconductance states (Lühring, 1986; Tyerman, Findlay & Terry, 1989). They are activated by voltage (Laver & Walker, 1987) and by micromolar cytosolic Ca^{2+} (D.R. Laver, *unpublished data*). The kinetics of ion permeation through these K^+ channels are similar to those found in animal maxi-K channels (Laver et al., 1989), which have been well studied in animal cells (e.g., Latorre et al., 1989). The K^+ current in this channel is limited by diffusion of K^+ from the bulk aqueous phases to the pore mouths (diffusion-limited) (Laver et al., 1989). Analysis of Na^+ block in maxi-K channels in bovine chromaffin cells (Yellen, 1984*a*) is also consistent with diffusion-limited K^+ flow in this channel.

The patch-clamp technique is used here to measure the effects of Ca^{2+} on the ion-gating and permeation characteristics of single maxi-K channels in drop-attached and excised inside-out membrane patches. These effects are analyzed within the framework of Läuger's (1976) theory of diffusion-limited ion flow and Läuger's (1973) rate theory approach to ion permeation. This theory is described in the Appendix. The voltage-dependent gating of the *Chara* channel has been modelled (Laver & Walker, 1987) by a kinetic scheme which includes two voltage-dependent gating mechanisms.

Ca^{2+} blockade of the channel is analyzed here in terms of the Woodhull model of voltage-dependent ion block (Woodhull, 1973), a model previously applied to K^+ channels in the plasmalemma of *Chara* by Tester (1988). The interaction of Ca^{2+} with the channel's gating mechanisms is used here to probe the structure of the channel, to refine the ion-gating model, and to provide it with some physical basis.

Materials and Methods

Cytoplasmic drops were formed from the internodal cells of *Chara australis* R. Br. using the method of Kamiya and Kuroda (1957). During experiments on drop-attached patches the composition of the medium bathing the cytoplasmic drops was usually

150 mol/m^3 KCl, 0.5–5 mol/m^3 $CaCl_2$. The blocking effect of external [Ca^{2+}] in drop-attached and excised inside-out patches was studied by comparing single channel recordings from pipettes containing different [Ca^{2+}]. Ion block due to internal [Ca^{2+}] was achieved using excised inside-out patches and by varying [Ca^{2+}] in the bath. Experiments were performed at 23 ± 2°C.

Details of the patch pipette fabrication, experimental protocol and the recording and display apparatus have been described previously by Laver and Walker (1987) and Laver et al. (1989). Micropipettes were made from borosilicate glass (Vitrex BRI/E) or from the same with an internally fused filament (Intrafil 01-003-06). Upon achieving a high resistance seal (10–50 GΩ) between the membrane patch and the micropipette, the pipette potential was clamped to a random sequence of values over the range −200 to 300 mV at 10–100 sec intervals. The method for calculating the potential difference across the membrane patch (V_m), taking into account the liquid-junction potential, is given by Laver et al. (1989). The time course of the transmembrane current and pipette potential were recorded simultaneously on video tape using Pulse Code Modulation encoding. The current signal was recorded with a bandwith of 10 kHz. The current and voltage recordings were later digitized and redisplayed graphically using a cathode ray oscilloscope. Unitary currents were measured from the size of the current steps. The calibration of the recording system was made by recording a square waveform with 5 volt amplitude.

Frequency distributions of channel open and closed durations were compiled from single channel recordings using the software package IPROC2 (from Dr. C. Lingle, Department of Biological Sciences, Florida State University). Allowance was made for unresolved events using the method of Blatz and Magleby (1986). Theoretical event duration frequency distributions were calculated using the theory of Colquhoun and Hawkes (1981, 1982). The kinetic analysis of the single-channel recordings is discussed further by Laver and Walker (1987).

Results

Single channel recordings on cell-attached patches shown in Fig. 1 illustrate the two main effects of external Ca^{2+} on maxi-K channel currents. First, Ca^{2+} significantly reduces the unitary-current at negative membrane potentials which is presumably the mean effect of fast, unresolved blocking events. Second, Ca^{2+} causes a "flicker block" which arises from blocking events that are of sufficient duration to be partially resolved by the recording apparatus. These are prominent at potentials more negative than −150 mV.

The attenuating action of external Ca^{2+} on the K^+ current in drop-attached and excised inside-out patches is shown in Fig. 2*a,b*. Variation in this data between different patches is less than ± 1 pA. The reproducibility is sufficiently good to allow comparison of data obtained from different patches. The reversal potentials of the current-voltage (*I/V*) curves are consistent with [K^+] = 100–120 mol/m^3 in the cytoplasm of the drop. The current has a nonlinear dependence on membrane potential and [K^+].

The effect of external Ca^{2+} on the gating kinetics of K^+ channels in drop-attached patches is shown in Figs. 3 to 5. At low external [Ca^{2+}] the frequency distribution of open times (Fig. 3*a*) could be adequately fitted by a single exponential with a voltage-dependent time constant, τ_o, ranging from 0.1 to 10 msec and showing a maximum between −100 to −150 mV. The occasional presence of a second small exponential component could be discerned in the open time distributions at short times ($t < 0.5$ msec, *see* Fig. 3*a*). This result was also reported previously (Laver & Walker, 1987) where it was interpreted as an artifact of background signal noise producing false channel events. However, since then it has been found (*unpublished data*) that an alternate event detection technique of Vivaudou, Singer and Walsh (1986) also generates similar open time frequency distributions. Therefore, it appears that this is not merely an artifact of the event detection software.

The frequency distribution of closed times is also voltage dependent. At least three exponential components with time constants over the range 0.1 to 100 msec could be discerned as distinct shoulders in the frequency distributions shown in Fig. 3*b*.

The Ca^{2+}-induced flicker block is manifest as an additional exponential component in the closed duration frequency distribution (*see* Fig. 4), which has a voltage-dependent time constant (0.2 msec at V_m = −250 mV). The magnitude of the Ca^{2+}-induced exponential component increases with increasing [Ca^{2+}] and with more negative membrane potentials but is reduced by increasing [K^+]. The data in Fig. 5 shows that Ca^{2+} also reduces the mean open duration of the channel.

The effect of cytosolic Ca^{2+} on the K^+ channels in excised inside-out patches is shown in Fig. 6. Cytosolic Ca^{2+} also reduces the K^+ current through the channel. The cytosolic side of the pore is more sensitive to Ca^{2+} block than the outside; a 50% blockade of the pore is produced by cytosolic [Ca^{2+}] of 0.1–0.5 mol/m^3, whereas external [Ca^{2+}] must be 20 mol/m^3 to produce the same effect.

Discussion

The Model for Fast Ca^{2+} Blockade in a Diffusion-Limited Channel

The effect of Ca^{2+} on the *I/V* characteristics (i.e., the fast blocking kinetics) of the Ca^{2+}-activated K channel is analyzed here in terms of a model developed by Laver et al. (1989). Briefly, in this model it was assumed that the pore has single ion occupancy

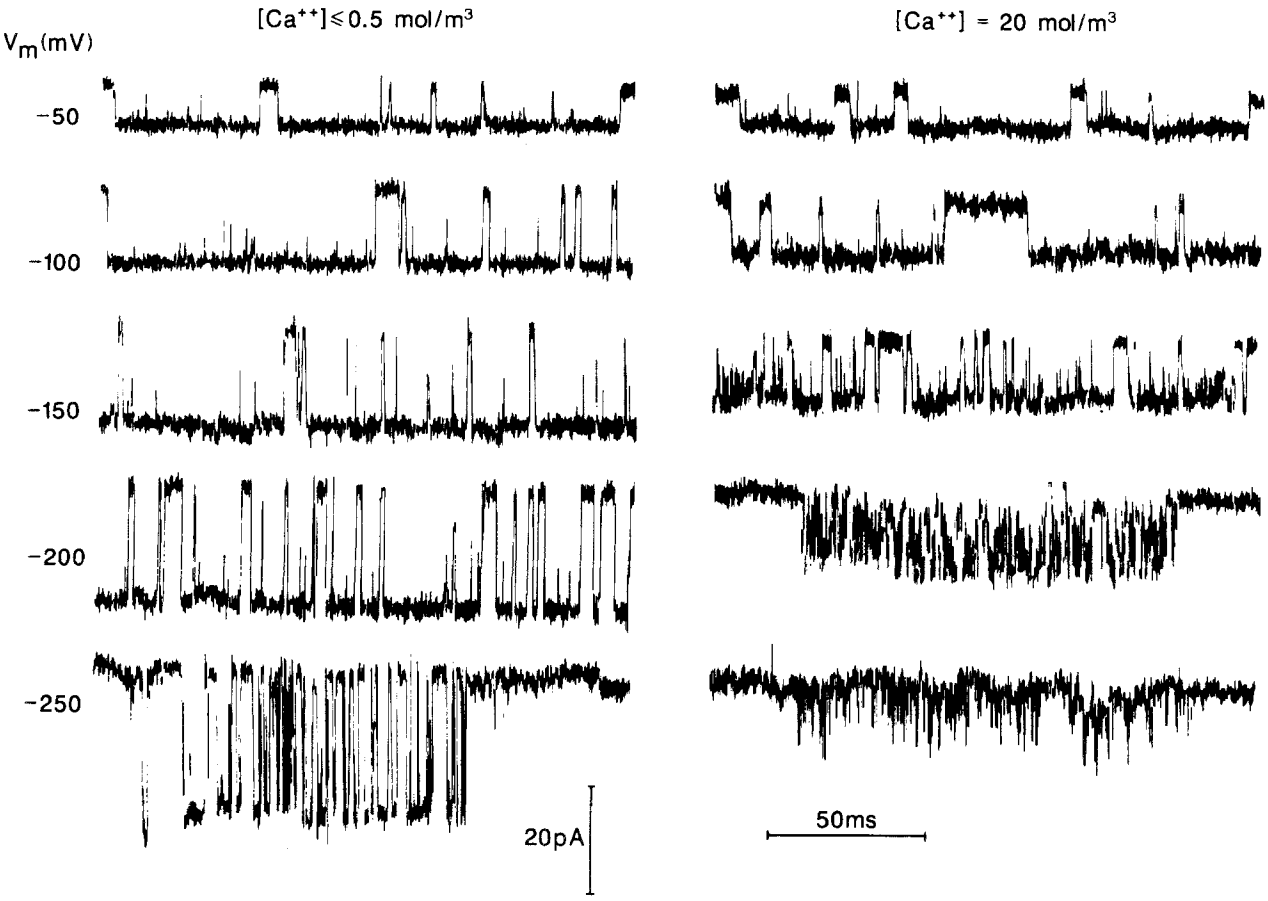

Fig. 1. Single channel recordings of maxi-K channels in drop-attached membrane patches at different membrane potentials, V_m. The frequency resolution shown here is 10 kHz. The zero conductance level is toward the top of each recording. The effect of external Ca^{2+} can be seen here as a reduction in the amplitude of the current fluctuations as well as the onset of a "flicker block" of the channel at more negative V_m

and that K^+ translocation through the pore is by electrodiffusion. Thus Läuger's (1973) rate theory approach was used to model K^+ permeation through the channel using an infinite number of uniform energy barriers (i.e., in the electrodiffusion limit). Diffusion of K^+ from the bulk phases to the pore mouths was found to limit the K^+ current through the channel, and Läuger's (1976) theory of diffusion-limited ion flow in a neutral pore was used to model these effects. The permeation coefficients, P_c' and P_c'', of the aqueous regions where the current paths converge and diverge (aqueous convergence regions) predicted by Läuger's (1976) model were found to be dependent on the ionic strength of the bulk solutions. This anomaly was believed to be a consequence of the inability of Läuger's model of a neutral cylindrical pore to model real, charged pores (Jordan, 1987). Therefore in this model, P_c' and P_c'' were given an ionic strength dependence described by the empirical equations (A28) and (A29) (*see* Appendix).

Two models for Ca^{2+} blocks are considered in this paper, competitive and noncompetitive. The competitive model (Model A) assumes that Ca^{2+} and K^+ cannot occupy the pore simultaneously, whereas the noncompetitive model (Model B) assumes that Ca^{2+} binding is unaffected by the presence of K^+ in the pore. Both kinetic schemes are based on the Woodhull (1973) model of voltage-dependent ion block, and assume that Ca^{2+} blocks the channel by binding to sites near each pore mouth (*see* Fig. 7). The two sites are assumed to be separated by a large energy barrier so that each site is accessible to Ca^{2+} from only one side of the pore. The binding sites are located a fraction of the distance through the pore, δ_1' and δ'', from the external and cytosolic sides, respectively.

Full details of the theory of ion permeation and blockade in a diffusion-limited pore is given in the Appendix. The application to the present model is summarized by Eqs. (A17)–(A19). The unknown

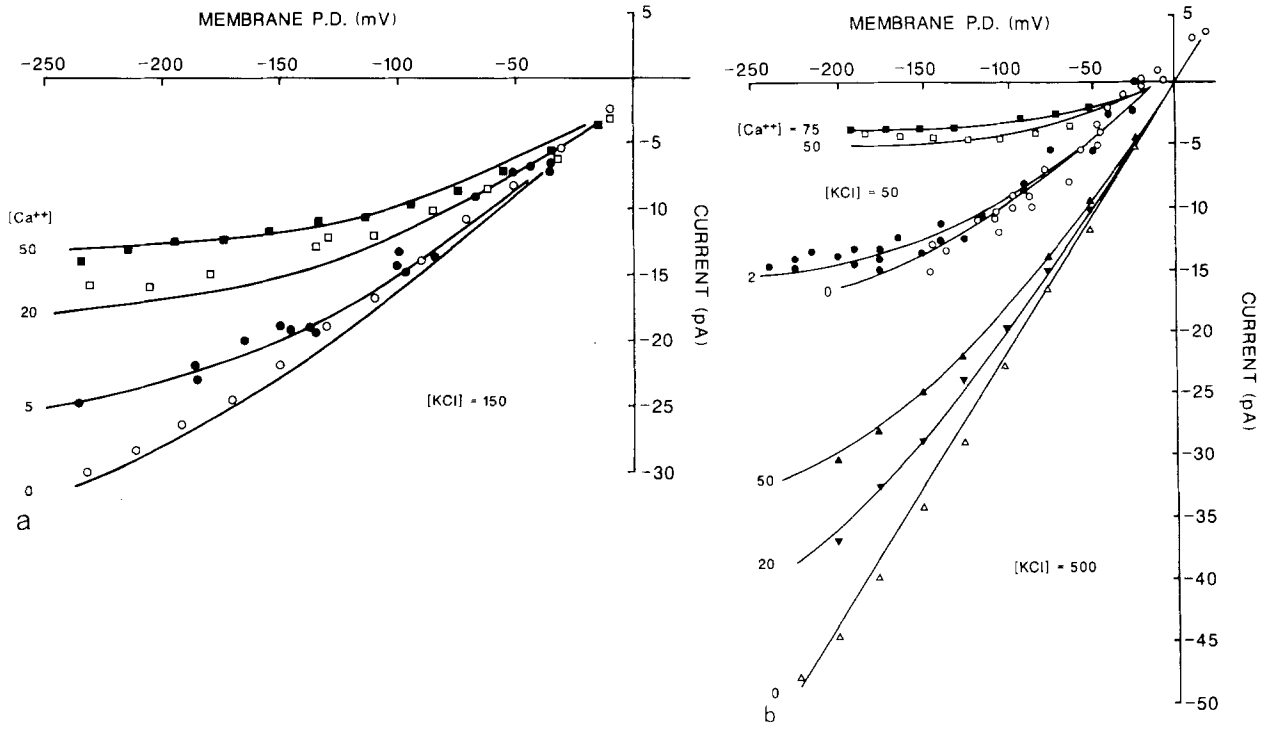

Fig. 2. (*a*) Typical *I/V* characteristics from several maxi-K channels in cell-attached patches with [KCl] = 150 mol/m^3 in the pipette. The ion concentrations are expressed in mol/m^3. Calcium concentrations in the diagram refer to those in the pipette. Symbol-[Ca^{2+}] (number of patches shown): ○—0.5 (1); ●—5 (6); □—20 (1); ■—50 (1). The solid curves are predictions of the theoretical model in the Appendix. The parameters of this fit are given in Table 1. (*b*) Typical *I/V* characteristics from several maxi-K channels in cell-attached patches with [KCl] = 50 mol/m^3 and excised inside-out patches in symmetric [KCl] = 500 mol/m^3. Symbol—[K^+], [Ca^{2+}] in mol/m^3 (number of patches shown): ○—50,0 (3); ●—50,2 (5); □—50,50 (1); ■—50,75 (1); △—500,0 (1); ▼—500,20 (1); ▲—500,50 (1). Parameters of the theoretical fit are the same as those in *a*

variables y', y'', and J were calculated by solving these simultaneous equations. Model values of current ($I = FJ$) were fitted to the data by varying the model parameters, described in the caption to Table 1. The best fits were established using the least-squares criterion and were found by the method of steepest descent. The two Ca^{2+} binding models were fitted with the data from Figs. 2*a*, 2*b* and 6 as well as data for the *I/V* characteristics of the channel for [KCl] over the range 10 to 500 mol/m^3 (Fig. 2 in Laver et al., 1989). The competitive kinetic scheme, Model A, appears to best account for the *I/V* characteristics of the channel; first, because Model A gives a better fit to the data than does Model B; and second, because Model B predicts a physically unreasonable location for the Ca^{2+} binding site (i.e., $\delta_1' < 0$). The binding site for external Ca^{2+} is relatively superficial being located approximately 8% of the electrical distance through the pore. Binding of cytosolic Ca^{2+} is much stronger than that of external Ca^{2+} as shown by the binding affinities in Table 1. The binding constants and effective location of the cytosolic binding site both depend on [Ca^{2+}] which indicates that the Ca^{2+} block on the cytosolic side of the channel is a multi-ion process and so must be modelled by a more complicated kinetic scheme than used here. Multi-ion binding behavior is commonly observed in maxi-K channels (Eisenman, Latorre & Miller, 1986; Cecchi et al., 1987).

Asymmetry in the *I/V* Characteristic

The *I/V* characteristics of the channel, in symmetric KCl solutions, were previously found to be asymmetric (Laver et al., 1989), the current being smaller at positive membrane potentials. This can be explained either by asymmetry in the energy barrier profile within the pore (e.g., Tyerman & Findlay, 1989) or by asymmetry in the aqueous convergence regions (e.g., Yellen, 1984*a*). Ion permeation models based on these two mechanisms will explain the observed Ca^{2+} block in terms of different Ca^{2+} binding kinetics. Therefore, it is necessary to identify the more likely cause of this asymmetry. Both possibilities have been consid-

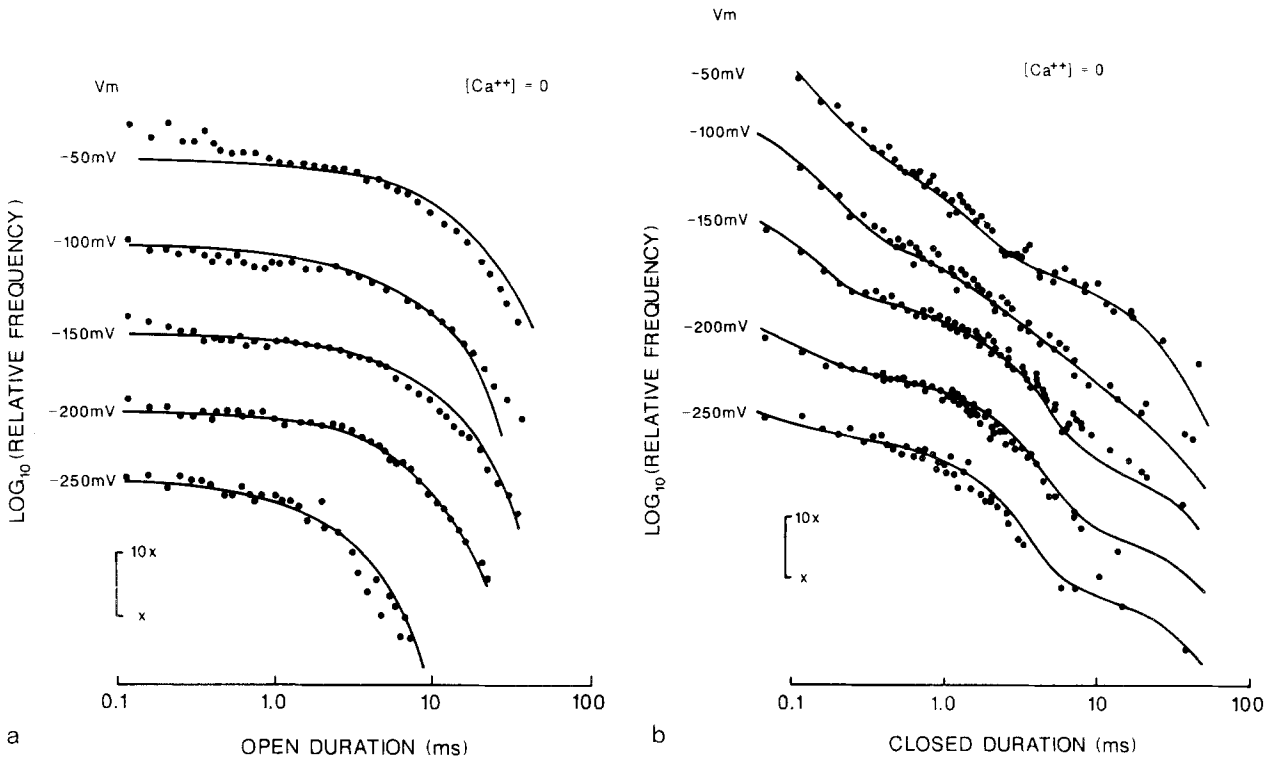

Fig. 3. (*a*) An example of the frequency distributions of open durations obtained from a single channel at different membrane potentials, V_m at low external $[Ca^{2+}]$. The solid curves are predictions of the model (Scheme 3) using the rate constants in Table 3. Note the presence of a second exponential component present in the data which can be detected as a small deviation from the model prediction at short times ($t < 0.5$ msec). (*b*) The frequency distributions of closed durations for the same channel as in *a*

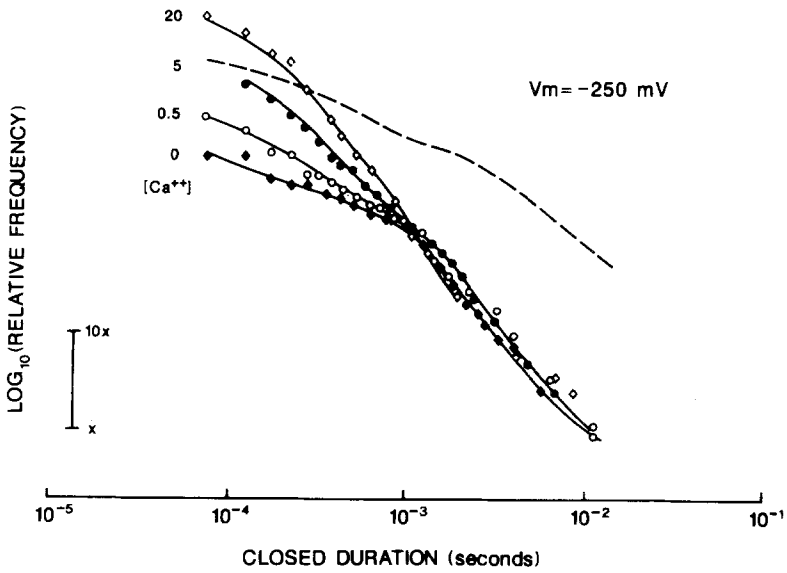

Fig. 4. The effect of varying $[Ca^{2+}]$ on the closed time distributions of channels in four different patches. The solid curves are predictions of kinetic Scheme 4 using the parameters in Table 3. The dashed line represents the predicted effect of 20 mol/m^3 external Ca^{2+} based on the data at $[Ca^{2+}] = 0$ and kinetic Scheme 5. Predictions of kinetic Schemes 5 and 6 are similar

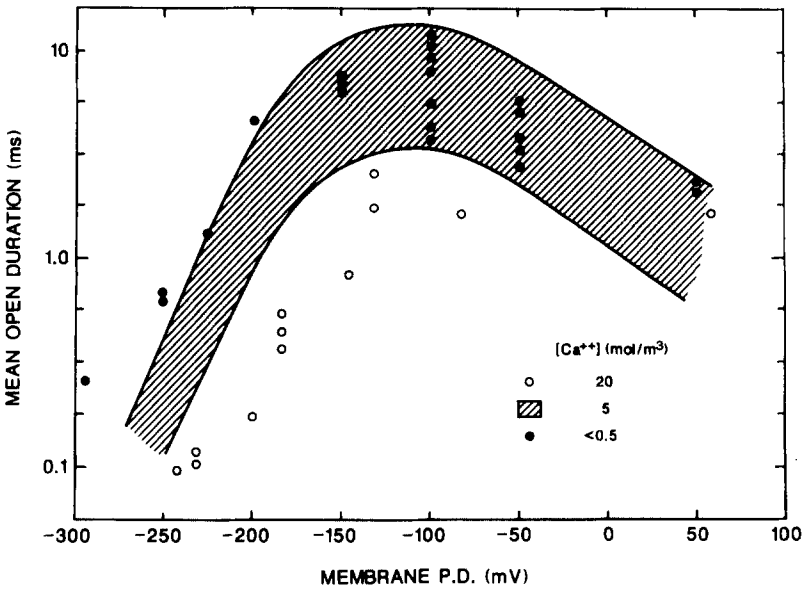

Fig. 5. The voltage dependence of the mean open duration for the channel in drop-attached patches with different $[Ca^{2+}]$ (mol/m^3) in the pipette. The shaded area is bordered by the 90% confidence limits of the distribution of 75 datum points

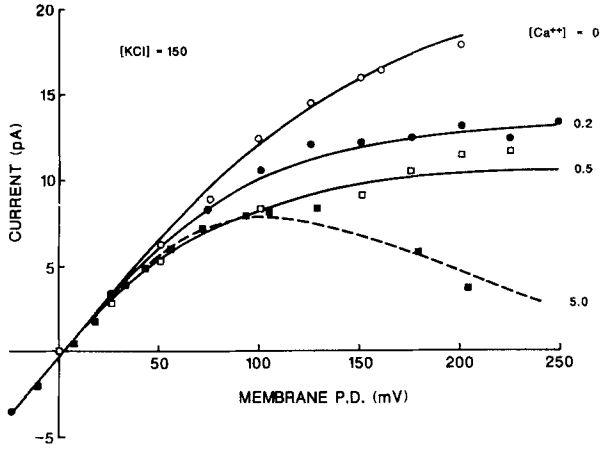

Fig. 6. The *I/V* characteristic of maxi-K channels in excised inside-out patches in symmetric [KCl] (mol/m^3). Symbol—$[Ca^{2+}]_{bath}$,$[Ca^{2+}]_{pipette}$ (in mol/m^3) (number of patches shown): ○—$<10^{-2}$, 5 (3); ●—0.2, 0, 2 (3); □—0.5, 0.5 (2); ■—5, 5 (2). The curves are fits of the theory in the Appendix to the data. The solid and dashed lines are derived from different sets of Ca^{2+} binding parameters applicable to high and low $[Ca^{2+}]$ (*see* Table 1)

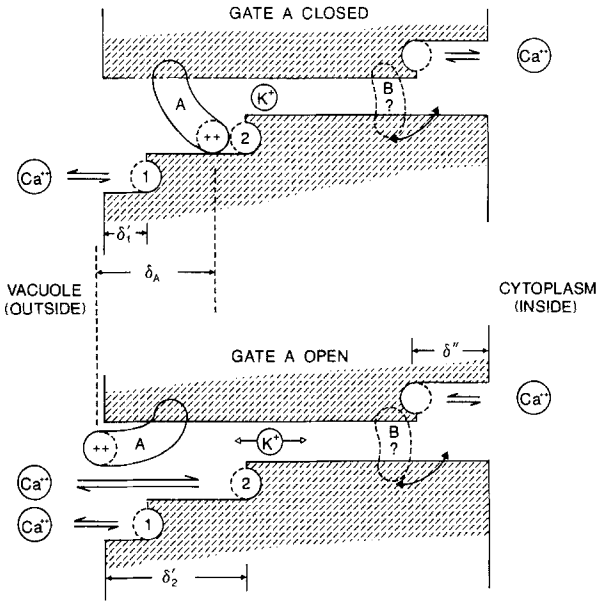

Fig. 7. A schematic diagram which outlines the main features of the model for Ca^{2+} block in this K^+ channel. Two Ca^{2+} binding sites are exposed to the outside face of the pore, Site *1* and Site *2*. The binding parameters for these sites are given in Tables 1 and 3. The external vestibule of the pore can be occupied by only one ion (Ca^{2+} or K^+). Site *2* is accessible by Ca^{2+} only when *Gate A* is in the open position. Operation of *Gate A* involves the movement of at least two positive charges through $\delta_A = 0.3$ of the trans-pore potential. The binding of Ca^{2+} from the outside solution to Sites *1* or *2* involves movement through $\delta'_1 = 0.08$ and $\delta'_2 = 0.4$, respectively, of the PD across the pore. Blocking of cytosolic Ca^{2+} is modelled here by a binding site accessible to the inside face of the pore and located at a "depth" of δ''. The value of δ'' is concentration dependent (*see* text). At present little can be said about the location and properties of *Gate B*

ered here and it is found that the latter gives the best account for the shape of the *I/V* characteristic. The problem with models based on asymmetry within the pore is that they predict the greatest curvature of the *I/V* characteristic at about 0 mV. However, a lower aqueous convergence permeability at the cytosolic pore mouth (*see* Table 2) could explain both the smaller current and increased curvature of the *I/V* characteristic at positive potentials as observed.

Table 1. Comparison of two models for K^+ permeation and rapid Ca^{2+} block

Model parameters	Units	Model A	Model B
$K_{m,K}$[a]	mol/m^3	46 ± 12	110 ± 26
$G_{max,K}$[b]	pS	343 ± 13	536 ± 40
$K'_{mCa,1}$[c]	mol/m^3	33 ± 11	66 ± 15
δ'_1[d]		0.081 ± 0.02	−0.026 ± 0.022
K''_{mCa}[c]	mol/m^3	0.5 ± 0.04[e]	—
		15 ± 5[f]	
δ''[d]		0.07 ± 0.04[e]	—
		0.27 ± 0.04[f]	
P'_∞[g]	× 10^{-18} m^3/sec	1.58 ± 0.14	0.975 ± 0.06
A'[g]		2.86 ± 0.6	5.36 ± 1.1
B'[g]	mol/m^3	63 ± 11	67 ± 8
P''_∞[g]	× 10^{-18} m^3/sec	0.507 ± 0.03	0.053 ± 0.04
A''[g]		8.37 ± 3.7	17.5 ± 10
B''[g]	mol/m^3	60 ± 11	44 ± 12
Residuals	pA (rms)[h]	1.03	1.5

The parameter values resulting from the least-squares fit of two models of rapid Ca^{2+} blockade of a diffusion-limited pore are shown. Model A assumes that K^+ and Ca^{2+} compete with each other for occupancy of the pore. Model B assumes noncompetitive binding of Ca^{2+} to the pore (i.e., that Ca^{2+} binding is unaffected by the presence of K^+ in the pore). These two models are fitted with the data in Figs. 2*a*, 2*b* and 6 as well as the data in Fig. 2 of Laver et al. (1989) (417 datum points in all). The errors indicate 90% confidence limits. The equations describing Ca^{2+} and K^+ permeation are given in the Appendix (Eqs. (A17) to (A29)).

[a] $K_{m,K} = K_K^{-1}$ is the binding affinity for K^+ in the channel.

[b] $G_{maxK^+} = F^2 k'_o/RT$ is the K^+ conductance of the channel symmetric high [K^+] in the absence of blocking ions.

[c] $K'_{mCa,1} = K'^{-1}_{Ca}$ and $K''_{mCa} = K''^{-1}_{Ca}$ are the binding affinities of external and internal Ca^{2+}, respectively.

[d] The depth (an electrical distance) of the Ca^{2+} binding sites within the pore from each pore mouth, expressed as a fraction of the pore length. ′ and ″ superscripts indicate the sites accessible from the external or cytosolic bulk phases, respectively.

[e] Binding parameters for cytosolic Ca^{2+} when [Ca^{2+}] = 0.2 and 0.5 mol/m^3.

[f] Binding parameters for cytosolic Ca^{2+} when [Ca^{2+}] = 5 mol/m^3.

[g] The parameters describing the dependence of the effective permeation constants of the aqueous convergence regions, P_c, on the ionic strength of the bulk phases (*see* Eqs. (A28) and (A29)). The ionic strength dependence of P_c for model A is explicitly shown in Table 2.

[h] The root mean square of the differences between each permeation model and the data.

Table 2. [KCl]-dependence of the maxi-K channel permeation constants

[KCl]	P_K	P'_c	P''_c	P_K/P'_c	P_K/P''_c
mol/m^3	{	× 10^{-18} m^3/sec[a]	}		
0	1.93	6.10	4.75	0.32	0.41
10	1.59	5.44	4.10	0.29	0.39
20	1.35	4.87	3.55	0.28	0.38
50	0.92	3.62	2.35	0.25	0.39
100	0.61	2.50	1.31	0.24	0.47
150	0.45	2.00	0.86	0.23	0.52
200	0.36	1.77	0.66	0.20	0.55
500	0.16	1.58	0.51	0.10	0.31
∞	0	1.58	0.51	0	0

Shown are the values permeation constants for the pore, P_K, and aqueous convergence regions, P'_c and P''_c, predicted by Model A (*see* Table 1), over a range of [KCl]. The ratios of the permeation constants of the pore and the aqueous convergence regions increase with increasing importance of diffusion-limiting effects.

[a] The permeation constants are a product of (permeability · area) and so have the dimensions m^3/sec.

The Model for Slow Ca^{2+} Blockade: Ion-Gating Kinetics

The effect of external Ca^{2+} on the voltage-dependent gating kinetics (i.e., the Ca^{2+}-induced "flicker block") is analyzed within the framework of the kinetic model of Laver and Walker (1987). The main aspects of the development of their model are as follows. The exponential frequency distribution of channel open durations (Fig. 3*a*) indicates that there exists one open state[1] for this channel. The rate constants of the reaction scheme are expected to

[1] The presence of two exponential components in the open time frequency distributions indicate that there are two open states for this channel.The previously reported open state dominates the open-time frequency distributions, whereas the short-lived open state contributes to less than 5% of the open events and in many instances is difficult to discern from the frequency distributions. Therefore, in modelling the main aspects of the ion-gating kinetics, it suffices for the moment to only include one open state in the model.

vary exponentially with V_m. Therefore, the observed nonexponential voltage-dependence of the mean open time, τ_o, (Fig. 4) indicates that the channel is closed by at least two mechanisms (referred to here as Gate A and Gate B), which must have opposite voltage dependences. Thus the minimum kinetic scheme for the channel is Scheme 1*a*. However, if Gate A and Gate B operate independently, then this is described by Scheme 1*b*[2].

Scheme 1*a*: $\begin{matrix} A \rightleftharpoons O \\ \downuparrows \\ B \end{matrix}$ Scheme 1*b*: $\begin{matrix} A \rightleftharpoons O \\ \downuparrows \quad \downuparrows \\ AB \rightleftharpoons B \end{matrix}$

where A and B are groups of closed states for each gate, AB are states representing both gates closed and O is the open state. Laver and Walker (1987) argued that at very negative membrane potentials the reaction rate constants in group A would dominate the closed time distribution, whereas at positive membrane potentials those of group B would dominate. With this in mind, it was possible to fit the closed and open time distributions with an eight-state model in which there were four closed states in group A and three in group B. The interconnections between closed states within these groups were not discernible from that data, and so a linear configuration of closed states was arbitrarily chosen.

Scheme 2: $A4 \rightleftharpoons A3 \rightleftharpoons A2 \rightleftharpoons A1 \rightleftharpoons O \rightleftharpoons B1 \rightleftharpoons B2 \rightleftharpoons B3$

Scheme 2 was developed to describe the ion gating of this channel in drop-attached patches in the presence of 5 mol/m^3 external Ca^{2+}. When external $[Ca^{2+}]$ is varied, the model parameters change. The closed state responsible for most of the longest channel closures ($t > 50$ msec), A4, is now thought to be associated with activation of the channel by internal Ca^{2+} (*unpublished data*). Hence the connection between State A4 and the rest of kinetic Scheme 2 is currently being reviewed and so will not be considered here. Another state in Group A (actually A1) is associated with the flicker block by external Ca^{2+}, which is now under consideration. In the absence of external Ca^{2+}, therefore, a reduced six-state kinetic model is adequate to describe the frequency distribution of the channel closed durations over the range 0.05–50 msec.

[2] In the present case Schemes 1*a* and 1*b* predict virtually identical event frequency distributions (*data not shown*) and so it is not possible to distinguish between the two kinetic schemes based on the data in Figs. 3 to 5. Therefore, in order to greatly reduce the complexity of the kinetic models, hence the computer calculation time, the simpler gating scheme, Scheme 1a, is used here to model the data.

Scheme 3: $A2 \rightleftharpoons A1 \rightleftharpoons O \rightleftharpoons B1 \rightleftharpoons B2 \rightleftharpoons B3$

The rate constants associated with this reaction scheme are given in Table 3. The predictions of the model are compared with the data in Figs. 3*a* and *b*. The addition of external Ca^{2+} reduces τ_o and adds one additional exponential component to the frequency distribution of closed durations. This indicates that Ca^{2+} introduces another closing mechanism for the channel and that it binds to a single binding site.

Three alternative models for this are considered here. In the first model (Scheme 4) Ca^{2+} only binds when Gate A is open and Gate A cannot close while Ca^{2+} is bound within the channel. The second model (Scheme 5) assumes that Ca^{2+} can bind to the channel independently of Gate A (i.e., Ca^{2+} can bind to the open and closed states equally well). The third model (Scheme 6) accounts for the possibility that Ca^{2+}, when bound to the channel, can be trapped within the channel by closure of Gate A. Trapping of Ba^{2+} by maxi-K channels has been detected in patch-clamp experiments by Miller, Latorre and Reisin (1987). The interaction between Ca^{2+} and Gate B cannot be resolved because Gate B does not significantly affect the gating kinetics of this channel over the range of potentials where Ca^{2+} binding is evident. Therefore the interaction between Ca^{2+} and Gate B has not been included in the kinetic models.

Scheme 4: $\begin{matrix} A2 \rightleftharpoons A1 \rightleftharpoons O \rightleftharpoons B1 \rightleftharpoons B3 \\ \qquad\qquad\quad \downuparrows \\ \qquad\qquad\quad C \end{matrix}$

Scheme 5: $\begin{matrix} A2 \rightleftharpoons A1 \rightleftharpoons O \rightleftharpoons B1 \rightleftharpoons B2 \rightleftharpoons B2 \\ \downuparrows \quad \downuparrows \quad \downuparrows \\ C_{A2} \rightleftharpoons C_{A1} \rightleftharpoons C_O \end{matrix}$

Scheme 6: $\begin{matrix} A2 \rightleftharpoons A1 \rightleftharpoons O \rightleftharpoons B1 \rightleftharpoons B2 \rightleftharpoons B3 \\ \qquad\qquad\quad \downuparrows \\ C_{A2} \rightleftharpoons C_{A1} \rightleftharpoons C_O \end{matrix}$

Kinetic states labeled *C* represent states where Ca^{2+} is bound to the pore. In Schemes 5 and 6 the rate constants, $q_{i-j} = q_{ci-cj}$ (i and j representing all states), $q_{ci-i} = q_{cj-j}$ and $q_{i-ci} = q_{j-cj}$. Kinetic Scheme 4 was found to give the best and most economical fit to the data (Fig. 4). The only rate constant to show a $[Ca^{2+}]$ dependence in this model was that associated with Ca^{2+} binding. The rate constants for Ca^{2+} binding, q_{o-c}, and unbinding, q_{c-o}, follow opposite voltage dependences with approximately equal magnitude, suggesting a binding site for Ca^{2+} that is 30–40% of the way through the channel from the outside. The position of this Ca^{2+} binding site (Site 2, *see* Fig. 7) is quite distinct from that of the site (Site 1) responsible for the rapid Ca^{2+} block. The rate of Ca^{2+} binding was found to be approximately

Table 3. Reaction rate constants from state x to y, q_{x-y}: $a[,b]^*$ sec^{-1}

$[Ca^{2+}],[K^+]$ (mol/m^3)	0,150	0.5,150	5,150	20,150	20,500	50,150
x,y						
#[a]	3	2	5	3	1	2
A2,A1	50	40	150	200	200	100
A1,A2	100	140	100	60	100	150
A1,O	1000	1300	2000	1400	1800	1400
O,A1	4, −0.5	3, −0.6	5, −0.65	5, −0.65	5, −0.6	3, −0.6
O,B1	2000, 0.3	4000, 0.4	750, 0.25	2000, 0.3	1000, 0.25	1500, 0.25
B1,O	20000	16000	2400	20000	10000	20000
B1,B2	1200	1200	400	1200	2000	1500
B2,B1	1900, −0.1	1500	700, −0.29	1900, −0.1	700, −0.1	700, −0.29
B2,B3	400	330	150	400	300	400
B3,B2	100, −0.2	50, −0.22	70, −0.34	100, −0.2	100, −0.2	100, −0.2
O,C	<5, −0.38	5–30, −0.38	70–120, −0.38	500–800, −(0.3–.38)	200, −0.3	550–600, −0.35
$V_m = -200$ mV	<100	100–600	1500–2500	8000–10000	2200	9000–10000
Model	0	200	1800	6000	2400	11000
C,O[b]	6×10^5, 0.38	6×10^5, 0.38	6.5×10^5, 0.38	6×10^5, (0.3–0.38)	3.5×10^5, −0.3	6×10^5, 0.35
$V_m = -200$ mV			31,000	27,000–29,000	32,000	33,000

Summary of the values of the rate constants associated with kinetic Scheme 4 for representative maxi-K channels in different external $[Ca^{2+}]$ and $[K^+]$. The only rate constant that shows significant dependence on $[Ca^{2+}]$ is q_{O-C}. The rate of Ca^{2+} binding at $V_m = -200$ mV is compared with the predictions of a model for competitive ion binding (*see* Eq. (1)). The binding affinity parameters, $K_{m,K}$ and $K'_{mCa,1}$, used in Eq. (1) are calculated from the data in Table 1 ($K_{m,K} = 46$ mol/m^3 and $K'_{mCa,1} = 17$ mol/m^3. The binding affinity for Ca^{2+} for the deep site, $K'_{mCa,2} = 20$ mol/m^3.

* Voltage-dependent rate constants are expressed in the form $a \cdot \exp(b \cdot FV_m/RT)$.

[a] # refers to the number of patches from which the data in this Table are derived.

[b] When $[Ca^{2+}] \leq 0.5$ mol/m^3 the value for this rate constant is assumed to be approximately that for $[Ca^{2+}] > 0.5$ mol/m^3.

proportional to $[Ca^{2+}]$ over the range 0 to 20 mol/m^3 and could be significantly reduced by increasing $[K^+]$ or by $[Ca^{2+}]$ in excess of 20 mol/m^3. The rate constants for Scheme 4 are given in Table 3.

Kinetic Schemes 5 and 6 fitted poorly with the data. They predict that increased Ca^{2+} binding substantially increases the closed durations (*see* Fig. 4), an effect not apparent in the data. The physical basis for the difference between the predictions of Scheme 4 and Schemes 5 and 6 is that when $V_m = -250$ mV the mean open time of Gate A is relatively short (approximately 0.3 msec) and the mean duration of Ca^{2+} binding is approximately 0.2 msec. In Schemes 5 and 6 it is possible for Gate A to open and then close again while Ca^{2+} remains in the pore. This would have the effect of removing open intervals and adjoining closed intervals, thus giving rise to longer closed durations. However, Scheme 4 requires that the Gate A must open before Ca^{2+}-induced closures can occur, and so joining of adjacent closed intervals by Ca^{2+} block is not possible. Schemes 5 and 6 would not fit to the data without a considerable increase in the complexity of the $[Ca^{2+}]$- and voltage-dependent of the reaction rate constants.

The Effect of Diffusion-Limited Ion Flow on the Slow Ca^{2+} Block

While effects of diffusion-limitation of K^+ current have been included in the model describing the fast Ca^{2+} block, it has not been included in the modelling of the slow Ca^{2+} block. Consideration is given here to the diffusion-limitation effects on the Ca^{2+} binding at Site 2. The rate constants for ion binding and unbinding within the channel depend on the potential difference, PD, between the bulk phase and the ion binding site. In a diffusion-limited channel this can differ from the PD between the binding site and the pore mouth because of the potential drop that exists across the aqueous convergence regions outside the pore. When a blocking ion enters the channel the current ceases and the potential profiles outside the pore quickly decay away; the fraction of the transmembrane PD between the site and the bulk phases, δ, is thus reduced. The magnitude of this effect is largest at the pore mouth and is zero at some point deep within the pore. Yellen (1984*a*) used this idea to explain the large difference between the voltage dependences of Na^+ binding and unbinding in a maxi-K channel. Model A (*see* Table 1) predicts that δ for Ca^{2+} binding at Site 1 (20%) is larger than that for unbinding is (8%). However, at Site 2 this difference is insignificant (δ being 42% for binding and 40% for unbinding), and so diffusion-limitation effects need not be included in the analysis of Ca^{2+} binding at Site 2.

The Interaction of Ca^{2+} and K^+ at the External Face of the Pore

So far the kinetics of the fast and slow Ca^{2+} block have been considered independently. Two Ca^{2+}

binding sites have been identified at the external face of the pore; a superficial site (Site 1) responsible for the Ca^{2+}-dependent attenuation of the K^+ currents and a deep site (Site 2) giving rise to the Ca^{2+}-induced "flicker block." These sites are located at 8 and 40% of the way along the trans-pore potential, respectively (*see* Fig. 7).

In this section the results of the kinetic analysis of the fast Ca^{2+} block (Table 1) are integrated with those of the slow Ca^{2+} block (Table 3) to provide a more complete model for the ionic interactions at the external face of the pore. The kinetics of K^+ and Ca^{2+} binding are examined here for the case when $V_m = -200$ mV (*see* Table 3) where all the kinetic parameters are well determined. Table 3 shows that the Ca^{2+} binding rate is inhibited by increased external $[K^+]$ and $[Ca^{2+}]$ above 20 mol/m^3. This is indicative of a competition between Ca^{2+} ions and between K^+ and Ca^{2+} for the external face of the pore. If only a single Ca^{2+} or K^+ can occupy the pore then the rate of Ca^{2+} binding at Site 2 (q_{o-c} in Table 3) is related to the binding affinities of this site ($K_{m'Ca,2}$), the other Ca^{2+} site ($K_{m'Ca,1}$) and K^+ ($K_{m,K}$) by the following expression:

$$\frac{q_{o-c}}{q_{c-o}} = \left\{1 + \frac{[K^+]}{K_{m,K}} + \frac{[Ca^{2+}]}{K_{m'Ca,1}}\right\}^{-1} \cdot \frac{[Ca^{2+}]}{K_{m'Ca,2}}. \quad (1)$$

The terms in the parentheses represents the probability that the external face of the pore is not occupied by K^+ or Ca^{2+} at Site 1. The values for $K_{m,K}$ and $K_{m'Ca,1}$ are derived from the K^+ permeation model (Model A in Table 1). When $K_{m'Ca,2} = 20$ mol/m^3, the predicted binding rates for Ca^{2+} are in good agreement with the data (*see* Table 3). This result indicates that Ca^{2+} at Site 1 or K^+ within the pore prevents binding of Ca^{2+} at Site 2.

The rate of Ca^{2+} unbinding from Site 2 (*see* Table 3) is independent of $[Ca^{2+}]$, which implies that it is also independent of the occupancy of Site 1. This indicates that Ca^{2+} at Site 2 is not trapped by superficially bound Ca^{2+} at Site 1. Together with the fact that Ca^{2+} at Site 1 prevents Ca^{2+} binding at Site 2 (*see above*), it follows that Ca^{2+} does not bind at Site 1 while Site 2 is occupied. Therefore, two Ca^{2+} ions cannot simultaneously occupy the external vestibule of the channel.

It is well known that maxi-K channels allow several monovalent cations to interact within the pore simultaneously (e.g., Yellen, 1984*b*; Eisenman et al., 1986; Cecchi et al., 1987). However, the K^+ permeation characteristic and block by external Ca^{2+} of the Ca^{2+}-activated K channel in *Chara* indicates that only a single ion can occupy the external vestibule of the channel. Similarly, the blocking maxi-K channel from skeletal muscle by Ba^{2+} was found to behave like a single-ion process (Vergara & Latorre, 1983). This is not surprising since the stronger repulsive forces associated with divalent ions will more effectively prevent more than one ion occupying the confines of the pore than would monovalent ions.

Structural Implications

The model for Ca^{2+} binding at Site 2 (Scheme 4) predicts that this site is inaccessible to Ca^{2+} when Gate A is closed (*see* Fig. 7). This indicates that Gate A is on the external site of the channel and that Site 2 is located between the K^+-selective filter and Gate A. The inability of Gate A to close while Ca^{2+} is in the pore suggests that closure of the gate may involve movement of positive charge into the pore. The voltage-dependent kinetics of Gate A can be explained by the product $z\delta_A = 0.6$. Where δ_A is the electrical distance through which z positive charges move between the open and closed states of the gate. Since δ for Ca^{2+} binding at the deep site is less than 0.4 and δ_A should be smaller than this, it appears that the kinetics of Gate A involves the movement of more than one positive charge. The greater voltage dependence of the gate closing rate over its opening rate (*see* Table 3) suggests that the energy barrier encountered by Gate A is asymmetric with its maximum being located nearest to the closed gate position.

This study has not revealed much about the properties of the other gating mechanism (Gate B). However, Gate B may represent a similar gating mechanism to that referred to in a study of Ba^{2+} block in a maxi-K channel (Miller et al., 1987), which indicated the existence of a voltage-dependent gate at the cytosolic side of the channel. Miller et al. (1987) also suggested that a gate may exist at the external side of the channel, a suggestion which is confirmed by this study.

A crude estimate of the pore diameter at each pore mouth can be derived from the sum of K^+ capture radii of the pore and K^+ ionic radius (Läuger, 1976). The capture radii are calculated here from P_c' and P_c'' at high ion concentrations (Laver et al., 1989; *also see* Eq. (A6)) using an ion diffusion coefficient, $D = 10^{-9}$. The capture radii r' and r'' are 0.25 and 0.08 nm, respectively, which are similar to those of the maxi-K channel in chromaffin cells (Yellen, 1984*a*). Assuming the radius of K^+ is 0.15 nm, it appears that the external pore mouth diameter (0.8 nm) is larger than that on the cytosolic side of the channel (0.46 nm).

Conclusion

The K^+ permeation and gating characteristics of the Ca^{2+}-activated K channel in *Chara* are altered by the presence of Ca^{2+} on either side of the channel. Two mechanisms for block by external Ca^{2+} have been identified. First, external Ca^{2+} reduces the observed conductance of the channel by binding to a relatively superficial site, sensing approximately 8% of the transpore PD. Second, binding of external Ca^{2+} to a deep site which senses 40% of the transpore potential difference produces short interruptions in the K^+ current (flicker block) which are resolved by the patch-clamp apparatus. The kinetics of these two blocking effects indicate that the external vestibule of the channel can be occupied by at most one ion (K^+ or Ca^{2+}). Internal Ca^{2+} block of the channel is not consistent with models that assume single ion occupancy of the channel.

The K^+ channel possesses two voltage-dependent gating mechanisms with opposite voltage dependences. The one responsible for channel closures at negative membrane potentials (Gate A) is coupled with Ca^{2+} binding in such a way as to indicate that it is on the external side of the channel and that its closure involves the movement of positive charge (at least 2+, through 30% of the trans-pore PD) into the K^+ conduction pathway.

I wish to thank Prof. N.A. Walker for helpful discussions and for critically reading this manuscript. This work was supported by a QEII fellowship.

References

Barry, P.H., Diamond, J.M. 1980. Junction potentials, electrode standard potentials and other problems in interpreting electrical properties of membranes. *J. Membrane Biol.* **3**:93–122

Barry, P.H., Gage, P.W. 1984. Ionic selectivity of channels at the end-plate. *In:* Ion Channels: Molecular and Physiological Aspects. W.D. Stein, editor. Ch. 1, pp. 1–51. Academic, New York

Blatz, A.L., Magleby, K.L. 1986. Correcting single channel data for missed events. *Biophys. J.* **49**:967–980

Cecchi, X., Wolff, D., Alvarez, O., Latorre, R. 1987. Mechanisms of Cs^+ blockade in a Ca^{2+}-activated K^+ channel from smooth muscle. *Biophys. J.* **52**:707–716

Colquhoun, D., Hawkes, A.G. 1981. On the stochastic properties of single ion channels. *Phil. Proc. R. Soc. London B* **211**:205–235

Colquhoun, D., Hawkes, A.G. 1982. On the stochastic properties of bursts of single ion channel openings and of clusters of bursts. *Phil. Trans. R. Soc. London B* **300**:1–59

Eisenman, G., Latorre, R., Miller, C. 1986. Multi-ion conduction and selectivity in the high-conductance Ca^{2+}-activated K^+ channel from skeletal muscle. *Biophys. J.* **50**:1025–1034

Jordan, P.D. 1987. How pore mouth charge distributions alter the permeability of transmembrane ionic channels. *Biophys. J.* **51**:297–311

Kamiya, N., Kuroda, K. 1957. Cell operation in *Nitella*. I. Cell amputation and effusion of the endoplasm. *Proc. Jpn. Acad.* **33**:149–152

Latorre, R., Oberhauser, A., Labarca, P., Alvarez, O. 1989. Varieties of calcium-activated potassium channels. *Annu. Rev. Physiol.* **51**:385–399

Läuger, P. 1973. Ion transport through pores: A rate-theory analysis. *Biochim. Biophys. Acta* **311**:423–441

Läuger, P. 1976. Diffusion-limited ion flow through pores. *Biochim. Biophys. Acta* **455**:493–509

Laver, D.R., Fairley, K.A., Walker, N.A. 1989. Ion permeation in a K^+ channel in *Chara australis:* Direct evidence for diffusion limitation of ion flow in a maxi-K channel. *J. Membrane Biol.* **108**:153–164

Laver, D.R., Walker, N.A. 1987. Steady-state voltage-dependent gating and conduction kinetics of single K^+ channels in the membrane of cytoplasmic drops of *Chara australis*. *J. Membrane Biol.* **100**:31–42

Lühring, H. 1986. Recording of single K^+ channels in the membrane of cytoplasmic drop of *Chara australis*. *Protoplasma* **133**:19–27

Miller, C., Latorre, R., Reisin, I. 1987. Coupling of voltage-dependent gating and Ba^{2+} block in the high-conductance Ca^{2+}-activated K^+ channel. *J. Gen. Physiol.* **90**:427–449

Reeves, M., Shimmen, T., Tazawa, M. 1985. Ionic activity gradients across the surface membrane of cytoplasmic drops from *Chara australis*. *Plant Cell Physiol.* **26**:1185–1193

Sakano, K., Tazawa, M. 1986. Tonoplast origin of the membrane of cytoplasmic droplets prepared from *Chara* internodal cells. *Protoplasma* **131**:247–249

Tester, M. 1988. Potassium channels in the plasmalemma of *Chara corallina* are multi-ion pores: Voltage-dependent blockade by Cs^+ and anomolous permeabilities. *J. Membrane Biol.* **105**:87–94

Tyerman, S.D., Findlay, G.P. 1989. Current-voltage curves of single Cl^- channels which coexist with two types of K^+ channel in the tonoplast of *Chara corallina*. *J. Exp. Bot.* **40**:105–117

Tyerman, S.D., Findlay, G.P., Terry, B.R. 1989. Behaviour of K^+ and Cl^- channels in the cytoplasmic drop membrane of *Chara corallina* using a transient detection method of analysing single-channel recordings. *In:* Plant Membrane Transport: The Current Position. J. Dainty, M.I. De Michelis, E. Marre, and F. Rasi-Caldogno, editors. pp. 173–178. Elsevier, Amsterdam

Vergara, C., Latorre, R. 1983. Kinetics of Ca^{2+}-activated K^+ channels from rabbit muscle incorporated into planar bilayers: Evidence for a Ca^{2+} and Ba^{2+} blockade. *J. Gen. Physiol.* **82**:543–568

Vivaudou, M.B., Singer, J.J., Walsh, J.V., Jr. 1986. An automated technique for analysis of current transitions in multilevel single-channel recordings. *Pfluegers Arch.* **407**:355–364

Woodhull, A.M. 1973. Ionic blockage of sodium channels in nerve. *J. Gen. Physiol.* **61**:687–708

Yellen, G. 1984*a*. Ionic permeation and blockade in Ca^{2+}-activated K^+ channels of bovine chromaffin cells. *J. Gen. Physiol.* **84**:157–186

Yellen, G. 1984*b*. Relief of Na^+ block of Ca^{2+}-activated K^+ channels by external cations. *J. Gen. Physiol.* **84**:187–199

Received 4 January 1990; revised 27 March 1990

Appendix

Theory of Ion Blockade in a Diffusion-Limited Pore

Ion permeation through a pore will depend on both the rate of ion transport within the pore and the diffusion of ions between the bulk phases and the pore mouths. If the former is rapid enough, the diffusion of ions to the pore mouth will limit the current through the pore and the ion concentrations and electric potentials at the pore mouths will differ from those of the bulk phases in a current-dependent manner. Thus, the kinetics of ion blockade of such a pore will depend, among other things, on the magnitude and composition of the total current through the pore.

The appendix outlines a theoretical framework for the study of ion blockade in diffusion-limited channels. The theory is considered in three parts: First, ion diffusion outside the pore, where Läuger's theory (1976) for diffusion-limited ion flow is extended to consider more than one permeable ion species. Second, ion transport within the pore, derived using Läuger's (1973) rate theory approach. Third, the application of this theory to the present model for K^+ permeation through the maxi-K channel in *Chara*.

Ion Diffusion Outside the Pore

The theory of diffusion-limited ion flow through pores has been developed by Läuger (1976). He considered a simple geometrical model of a pore consisting of a right circular cylinder separating two aqueous phases. The current was assumed to converge and diverge with spherical symmetry at the pore entrances.

The aqueous phases (denoted by $'$ and $''$) contain m ion species (subscript i) each with a valency z_i. The ion concentrations, C_i' and C_i'', and electric potentials V (in units of F/RT) are related to the ion flux J_i by the Nerst-Planck equation, which is expressed here for each aqueous phase in radial symmetry.

$$\frac{J_i}{2\pi r^2} = D_i\left[\frac{dC_i'}{dr} + z_i C_i' \frac{dV}{dr}\right] \tag{A1}$$

$$\frac{J_i}{2\pi r^2} = -D_i\left[\frac{dC_i''}{dr} + z_i C_i'' \frac{dV}{dr}\right] \tag{A2}$$

(for $i = 1, 2, 3, \ldots m$).

When l different ion valencies Z_j are present, the solutions of Eq. (A1) and (A2) have the form

$$C_i' = \sum_{j=1}^{l} A_{ij}' \exp[-z_j(V - \Phi')] \tag{A3}$$

$$C_i'' = \sum_{j=1}^{l} A_{ij}'' \exp[-z_j(V - \Phi'')] \tag{A4}$$

(for $i = 1, 2, 3, \ldots m$).

Where Φ' and Φ'' are the electrostatic potentials in the bulk phases ($r = \infty$). Substituting Eqs. (A3) and (A4) into Eqs. (A1) and (A2) and then integrating the result between the limits $r = r_i'$ or $r = r_i''$ and $r = \infty$ gives

$$\frac{J_i}{P_{ci}'} = \sum_{j=1}^{l} A_{ij}'(1 - z_i/Z_j)(1 - y_i' - Zj) \tag{A5}$$

$$\frac{J_i}{P_{ci}''} = -\sum_{j=1}^{l} A_{ij}''(1 - z_i/Z_j)(1 - y_i'' - Zj) \tag{A6}$$

$$y_i' \equiv \exp(\Phi_{pi}' - \Phi')$$

and

$$y_i'' \equiv \exp(\Phi_{pi}'' - \Phi'')$$

$$P_{ci}' \equiv 2\pi r_i' D_i$$

and

$$P_{ci}'' \equiv 2\pi r_i'' D_i$$

(for $i = 1, 2, 3 \ldots m$)

where y_i' and y_i'' represent the Boltzmann factors for the partitioning of each ion species between the bulk phases and the mouths of the pore. Φ' and Φ'' (in units of F/RT) are the dimensionless electrostatic potentials at $r = \infty$. r_i' and r_i'' are the capture radii of the pore for each ion species which depend on both the geometry of the pore and the ionic radii. Variables subscripted with p indicate their respective values at $r = r_i'$ and $r = r_i''$ (i.e., at the pore mouth). P_{ci}' and P_{ci}'' are, effectively, the permeation constants of the aqueous convergence regions. The physical significance of these parameters is detailed by Läuger (1976).

To satisfy the electroneutrality assumption at every point outside the pore, the exponential coefficients A_{ij} for each ion species must be related by the following equations

$$\sum_{i=1}^{m} z_i A_{ij}' = 0 \tag{A7}$$

$$\sum_{i=1}^{m} z_i A_{ij}'' = 0 \tag{A8}$$

(for $j = 1, 2, 3 \ldots 1$).

The boundary conditions at $r = \infty$ provide the following equations:

$$\sum_{j=1}^{l} A_{ij}' = C_i' \tag{A9}$$

$$\sum_{j=1}^{l} A_{ij}'' = C_i'' \tag{A10}$$

(for $i = 1, 2, 3 \ldots m$).

In this way ion fluxes can be calculated without explicitly evaluating the electrostatic potentials at every point.

Ion Transport within the Pore

Ion permeation within the pore is derived here using the rate theory approach of Läuger (1973). We consider here m ion species competing for the pore which presents n_i sequential energy minima (binding sites) to the ion species i. The pore can be occupied by at most one ion.

Equation (A11) is taken from Eq. (22) of Läuger (1973) which is recast here to express the ion flux J_i in terms of the probability,

P, that the pore is occupied by an ion and the equilibrium binding constant for each ion species within the pore K_i.

$$J_i = \frac{k'_{oi}K_i}{\sum_{v=1}^{n} \bar{R}_{vi}} (1 - P) \frac{C'_{pi} - q_i C''_{pi}}{1 + \sum_{v=1}^{n} S_{vi}} \quad \text{(A11)}$$

$$1 - P = \left[1 + \sum_{i=1}^{m} B_i\right]^{-1} \quad \text{(competitive kinetics)} \quad \text{(A12a)}$$

$$1 - P = \left[\prod_{i=1}^{m} (1 + B_i)\right]^{-1} \quad \text{(noncompetitive kinetics)} \quad \text{(A12b)}$$

$$B_i = \frac{K_i(Q'_i C'_{pi} + q_i Q''_i C''_{pi})}{\sum_{v=1}^{n} \bar{R}_{vi}\left(1 + \sum_{v=1}^{n} S_{vi}\right)} \quad \text{(A13)}$$

$$q_i \equiv \exp(-z_i u_{pi})$$

$$u_{pi} \equiv \Phi'_{pi} - \Phi''_{pi}$$

where u_{pi} are the electrostatic potential differences between the pore mouths, defined by r'_i and r''_i. C_{pi} are the ion concentrations at the pore mouths. These parameters are related to the corresponding bulk phase parameters by the following equations:

$$C'_{pi} = \sum_{j=1}^{1} A'_{ij}(y'_i)^{-zj} \quad \text{(A14)}$$

$$C''_{pi} = \sum_{j=1}^{1} A''_{ij}(y''_i)^{-zj} \quad \text{(A15)}$$

$$u_{pi} = u + \ln(y'_i/y''_i). \quad \text{(A16)}$$

The voltage-dependent quantities, R_{vi}, Q_i, S_{vi}, and k'_{oi} are defined in terms of the energy profile within the channel for each ion species by Läuger, 1973.

Equation (A5) to (A16), for the following cases (when the number of unknowns, $(21 + 3) \cdot m$, is less than the number of equations, $(21 + 5m)$ can be solved to yield values for the total current, $\Sigma z_i F J_i$: (i) when only monovalent or divalent ions are present, and (ii) when both monovalent and divalent ions are present and only one ion species carries the current through the channel. With the approximations $y'_i = y'$ and $y''_i = y''$ (i.e., that the pore mouth electrostatic potentials are the same for each ion species) case ii can be extended to consider two permeable ion species.

Present Application of the Theory

The theory is applied here to the case of a pore which is permeable only to K^+ ($i \equiv K$) which competes with Ca^{2+} ($i \equiv Ca$) for entry into the pore. For this simple case (dropping the i subscript) Eqs. (A5) to (A10) reduce to the following two equations:

$$J/P'_c = 2C'_{Cl}(1 - y') + \tfrac{1}{2}C'_{Ca}(1 - y'^{-2}) \quad \text{(A17)}$$

$$J/P''_c = 2C''_{Cl}(1 - y'') + \tfrac{1}{2}C''_{Ca}(1 - y''^{-2}) \quad \text{(A18)}$$

The model assumes that the pore presents an infinite number of uniform energy barriers to K^+ permeation. The blocking effects of the impermeant Ca^{2+} ions are modelled with two binding sites (i.e., the pore presents three energy barriers to Ca^{2+}); each site being accessible from only one side of the pore (i.e., a large central energy barrier).

When n is large the predictions of the rate theory and the electrodiffusion model are the same (Barry & Gage, 1984). For large n Eqs. (A11) to (A16) become

$$J = u_p \cdot k'_o K_K (1 - P) \cdot (C'_{pK} - qC''_{pK})/(1 - q) \quad \text{(A19)}$$

where

$$1 - P = [1 + B_K + B_{Ca}]^{-1} \quad \text{(competitive block)} \quad \text{(A20a)}$$

$$1 - P = [(1 + B_K)(1 + B_{Ca})]^{-1} \quad \text{(non-competitive block)} \quad \text{(A20b)}$$

$$B_K = K_K[C'_{pK}\{1/(1 - q) + 1/u_p\} + C''_{pK}\{-1/u_p - q/(1 - q)\}] \quad \text{(A21)}$$

$$B_{Ca} = K'_{Ca}C'_{pCa}q^{(2\delta')} + K''_{Ca}C''_{pCa}q^{(-2\delta'')} \quad \text{(A22)}$$

$$C'_{pK} = C'_{Cl}y' - 2C'_{Ca}y'^{-2} \quad \text{(A23)}$$

$$C''_{pK} = C''_{Cl}y'' - 2C''_{Ca}y''^{-2} \quad \text{(A24)}$$

$$C'_{pCa} = C'_{Ca}y'^{-2} \quad \text{(A25)}$$

$$C''_{pCa} = C''_{Ca}y''^{-2} \quad \text{(A26)}$$

$$u_p = u + \ln(y'/y'') \quad \text{(A27)}$$

$$q \equiv \exp(u_p)$$

where K'_{Ca} and K''_{Ca} are the equilibrium constants for Ca^{2+} binding to the sites on each side of the pore. δ' and δ'' are the fractional electrical distances of the Ca^{2+} binding sites from outside the pore. The product, $k'_o K_K$, in Eq. (A19) presents the permeation constant pore the pore, P_K, in the limit of zero $[K^+]$.

In the present model the permeation constants of the aqueous convergence regions P'_c and P''_c depend on the ionic strength, I' and I'', of the bulk phase solutions (*see* Discussion). The ionic strength dependence is expressed by the following empirical equations:

$$P'_c = P'_\infty[1 + A' \exp(-I'/B')] \quad \text{(A28)}$$

$$P''_c = P''_\infty[1 + A'' \exp(-I''/B'')] \quad \text{(A29)}$$